Sensors and Materials, Vol. 37, No. 2 (2025) 617–626
MYU Tokyo

S & M 3942

Scintillation Properties of LiF/$(K_{0.75}Rb_{0.25})_2CuCl_3$ Composites for Thermal Neutron Detection

Noriaki Kawaguchi,* Keishi Yamabayashi, Kai Okazaki, Ryosei Takahashi, Takumi Kato, Daisuke Nakauchi, and Takayuki Yanagida

Nara Institute of Science and Technology, 8916-5 Takayama, Ikoma, Nara 630-0192, Japan

(Received November 12, 2024; accepted December 18, 2024)

Keywords: scintillator, thermal neutron, composite, radiation detection

LiF/$(K_{0.75}Rb_{0.25})_2CuCl_3$ composites were developed and their scintillation properties were investigated. Samples with mass ratios of LiF to $(K_{0.75}Rb_{0.25})_2CuCl_3$ of 1:3, 1:2, 1:1, 2:1, and 3:1 were prepared, and the 1:3 and 1:2 samples showed the highest signal intensity in the pulse height spectra under thermal neutron irradiation using ^{252}Cf. The signal intensities corresponded to light yields below 9000 photons/neutron. The estimated α/β ratio of the 1:3 sample was high (0.62), and the high α/β ratio characteristic was also observed in the commercial LiF/ZnS:Ag composite. The temperature dependence of X-ray-induced scintillation spectra from room temperature to 200 °C showed that the emission intensity of $(K_{0.75}Rb_{0.25})_2CuCl_3$ decreased more significantly at high temperatures than that of the lithium glass GS20.

1. Introduction

Radiation detectors equipped with scintillators are widely used in medical, industrial, and scientific applications. Scintillators are materials that emit light when excited by ionizing radiation, and their properties affect the performance of radiation detectors; therefore, research on various inorganic and organic scintillators has been conducted over the past couple of decades.[1–4] Novel materials have also been intensively studied, and various types of material such as single crystals,[5–22] crystalline films,[23] crystalline particles,[24] ceramics,[25–28] glasses,[29–39] and organic–inorganic hybrid materials[40,41] have been reported over the last few years. Single crystalline scintillators including NaI:Tl and Lu_2SiO_5:Ce are the most widely used among the reported scintillators, and they are grown by the melt growth method. On the other hand, research on single crystalline scintillators grown by the solution growth method has been attracting much attention. $(C_6H_5C_2H_4NH_3)_2PbBr_4$[42] has a high light yield and a short decay time, and is obtained by the antisolvent crystallization method, which is one of the solution growth methods. $Cs_3Cu_2I_5$-based scintillators[43] can be obtained by the melt growth method, as well as solution growth methods.[44]

Our group has also been studying single crystalline scintillators grown by a solution growth method, and we showed that $(K, Rb)_2CuCl_3$ single crystals,[45] which have a one-dimensional

*Corresponding author: e-mail: n-kawaguchi@ms.naist.jp
https://doi.org/10.18494/SAM5479

ISSN 0914-4935
https://myukk.org/

quantum confinement structure, showed high light yields from 12000 to 16000 photons/MeV under γ-ray irradiation and fast decay times of approximately 11–13 μs under X-ray irradiation. In addition, the $(K_{0.75}Rb_{0.25})_2CuCl_3$ single crystal showed the highest light yield among (K, Rb)$_2$CuCl$_3$ single crystals. We have been focusing on (K, Rb)$_2$CuCl$_3$ single crystals as an attractive candidate for novel scintillators; however, there has been a disadvantage that needle-like crystals are also naturally grown, making it difficult to produce the large single crystals required for γ-ray detection. Therefore, we investigated the use of $(K_{0.75}Rb_{0.25})_2CuCl_3$ as neutron scintillators.[46,47] The LiF/ZnS:Ag composite,[48] which is a combination of LiF and ZnS:Ag particles, and Ce-doped lithium silicate glass (Li-glass)[49] are widely used as neutron scintillators. Although the opaque LiF/ZnS:Ag composite has a lower neutron detection efficiency than transparent neutron scintillators including Li-glass owing to its small thickness, it is used in many applications because its low γ-ray detection efficiency leads to low measurement noise in neutron detection. Since composite neutron scintillators can be prepared without using large single crystals, we predicted that $(K_{0.75}Rb_{0.25})_2CuCl_3$ particles can be used as an alternative to ZnS:Ag particles. In this study, we prepared LiF/$(K_{0.75}Rb_{0.25})_2CuCl_3$ composites and investigated their properties.

2. Materials and Methods

A $(K_{0.75}Rb_{0.25})_2CuCl_3$ crystal was prepared by the solution growth method described in Ref. 45 by our group. The obtained crystal was ground with an alumina mortar and pestle, and mixed with LiF particles (99.9%, 95 mol% ^{6}Li; Sigma-Aldrich, USA) at mass ratios of LiF to $(K_{0.75}Rb_{0.25})_2CuCl_3$ of 1:3, 1:2, 1:1, 2:1, and 3:1, and then ground and mixed further with the alumina mortar and pestle. The mass ratio was used to express the mixture ratios because it is often used in research on the LiF/ZnS:Ag composite. Each obtained powder was filled into a metal mold (LD-1025; Labonect, Japan) with a diameter of 10 mm and pressed at 20 kN for 1 min using a hydraulic hand press machine (MP-100; Labonect). The obtained pressed samples had a strength sufficient to withstand handling with tweezers. It is possible that the robust pressed samples were obtained because halides are often plastically deformed.

The photoluminescence (PL) quantum yield of a part of the $(K_{0.75}Rb_{0.25})_2CuCl_3$ crystal, which was left uncrushed, was measured using a PL spectrometer (Quantaurus-QY; Hamamatsu Photonics, Japan) at 10 nm steps for comparison with that in the previous literature. In addition, the photoluminescence map of the obtained composite sample was measured using the same PL spectrometer to investigate whether any emissions other than that originating from the $(K_{0.75}Rb_{0.25})_2CuCl_3$ crystal were observed when it was composited with LiF. To examine the neutron detection capabilities of the composite samples, the pulse height spectra were measured under thermal neutron irradiation performed using a ^{252}Cf sealed source and a polyethylene moderator, and the emissions of the sample were detected by a photomultiplier tube (PMT; R7600U-200, Hamamatsu Photonics). The signals from the PMT were amplified and shaped using a preamplifier (Model 113; ORTEC, USA) and a shaping amplifier (Model 572; ORTEC), and analyzed using a multichannel analyzer (MCA8000A; Amptek, UK). To evaluate the discrimination performance between neutrons and γ-rays, the pulse height spectra under γ-ray

irradiation using ^{137}Cs and ^{60}Co sealed sources were also measured. The same measurements were performed on commercial LiF/ZnS:Ag (Ohyo Koken Kogyo, Japan) and Li-glass (GS20; Scintacor, UK) neutron scintillators for comparison.

Furthermore, to investigate whether the LiF/$(K_{0.75}Rb_{0.25})_2CuCl_3$ composite can be used as a neutron scintillator for well-logging applications, the temperature dependence of the scintillation intensity of the $(K_{0.75}Rb_{0.25})_2CuCl_3$ crystal was investigated. Since it is generally required that the light yield is sufficiently high up to approximately 200 °C,[50,51] the scintillation intensities were measured from room temperature to 200 °C. In practical applications, the light yield under neutron irradiation is important; however, we evaluated it using X-ray-excited scintillation spectra because the measurements were easily conducted. Figure 1 shows a schematic of these measurements. An AlN ceramic heater (WALN-3H; Sakaguchi Electric Heaters, Japan) was placed in an X-ray-shielding box (SBX001-NKK; ANSeeN, Japan), and samples were placed on it. X-ray irradiation was carried out using an X-ray generator (XMS-803 Type B; Kinki Roentgen Industrial) placed on top of the box while controlling the temperature with a power controller (SCR-SHQ-A2E; Sakaguchi Electric Heaters). The tube voltage and tube current during X-ray irradiation were set to 40 kV and 6 mA, respectively. The emission from the sample was transmitted through an optical fiber (F600-UVVIS-SR; StellarNet, USA) equipped with a fused silica collimating lens (74-UV, Ocean Insight, USA) at the tip facing the sample, and the spectrum was measured using a CCD spectrometer (SILVER-Nova; StellarNet). The spectrum was measured after the temperature was sufficiently stabilized, and the samples were irradiated with X-ray only during the spectrum measurement. The X-ray-excited scintillation spectra were measured from room temperature to 200 °C, and the integrated intensity was plotted against temperature. The integrated intensities were calculated as relative ratios, with the value at room temperature set to 1.

3. Results and Discussion

Figure 2(a) shows the PL quantum yield and absorption rate of the $(K_{0.75}Rb_{0.25})_2CuCl_3$ crystal. In Fig. 2(a), relatively strong optical absorption and emission of PL from the $(K_{0.75}Rb_{0.25})_2CuCl_3$ crystal were observed at wavelengths from 250 to 320 nm. High PL quantum yields from 80 to 90% were obtained at excitation wavelengths from 300 to 320 nm,

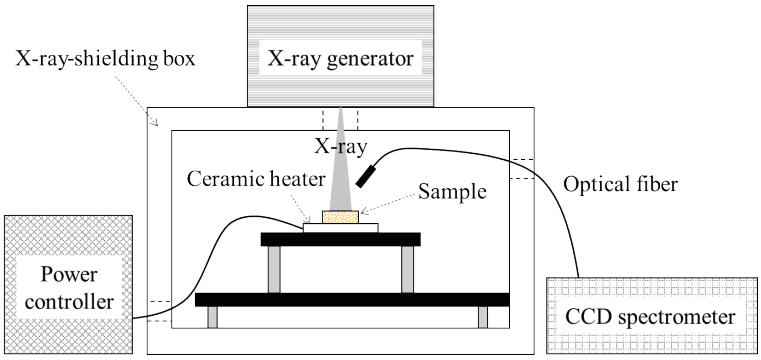

Fig. 1. (Color online) Experimental setup used in measurements to determine temperature dependences of X-ray-induced scintillation intensities.

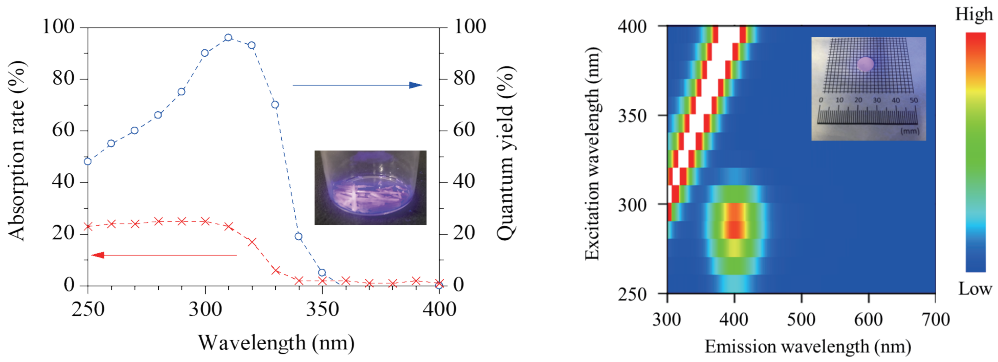

(a) (b)

Fig. 2. (Color online) (a) PL quantum yield and absorption rate of $(K_{0.75}Rb_{0.25})_2CuCl_3$ and (b) PL excitation and emission map of the 1:2 sample. Insets show the appearances of the measured samples under 302 nm UV excitation.

which is consistent with the previous report.[45] Figure 2(b) shows the PL excitation and emission map of the 1:2 sample, which means LiF:$(K_{0.75}Rb_{0.25})_2CuCl_3$ is 1:2. Although the emission attributable to the $(K_{0.75}Rb_{0.25})_2CuCl_3$ crystal was observed, no other emissions (for example, emissions attributable to LiF) were observed. This result indicates that the scintillation properties of the composite samples may mainly depend on those of $(K_{0.75}Rb_{0.25})_2CuCl_3$.

Figure 3(a) shows the pulse height spectra of all the obtained samples under thermal neutron irradiation using a ^{252}Cf sealed source and a polyethylene moderator. No full absorption peaks were observed. The spectral shapes are typical of an opaque composite scintillator, since the emitted light is scattered in the material, resulting in an inhomogeneous emission intensity. In addition, when the mass ratio of LiF and $(K_{0.75}Rb_{0.25})_2CuCl_3$ was different, the shape of the pulse height spectra under thermal neutron irradiation was also different. The samples with higher $(K_{0.75}Rb_{0.25})_2CuCl_3$ content tended to show signals corresponding to higher light yields; however, the shapes of the pulse height spectra were similar for the 1:2 and 1:3 samples. Therefore, they are considered to have appropriate mixing ratios for the LiF/$(K_{0.75}Rb_{0.25})_2CuCl_3$ composites. Figure 3(b) shows the pulse height spectrum of the 1:3 sample that showed the highest pulse height under thermal neutron irradiation using ^{252}Cf and the moderator, 0.662 MeV γ- rays from ^{137}Cs, and 1.173 and 1.333 MeV γ-rays from ^{60}Co. The pulse height spectrum under thermal neutron irradiation partially overlaps with that under γ-ray irradiation, but does not overlap in the high-channel-number region above 150 channels. This result indicates that it is possible to detect neutrons in the presence of γ-rays with energies lower than those of ^{60}Co using the 1:3 sample.

The pulse counts shown at the vertical axis in Fig. 3(a) were different depending on the mixture ratio of LiF and $(K_{0.75}Rb_{0.25})_2CuCl_3$, although these data were obtained under the same measurement conditions. The amount of neutron detection signals from the samples with higher LiF contents tended to be smaller. Since ^{6}Li in LiF absorbs neutrons, it is intuitively unnatural that the pulse count was lower in the samples with higher LiF contents. This is possibly because when the $(K_{0.75}Rb_{0.25})_2CuCl_3$ content is low, the energy of the particle radiation generated by the ^{6}Li(n, α)t reaction is not sufficiently absorbed by the small number of $(K_{0.75}Rb_{0.25})_2CuCl_3$ particles in the sample but is absorbed and lost by the large number LiF particles. In this case,

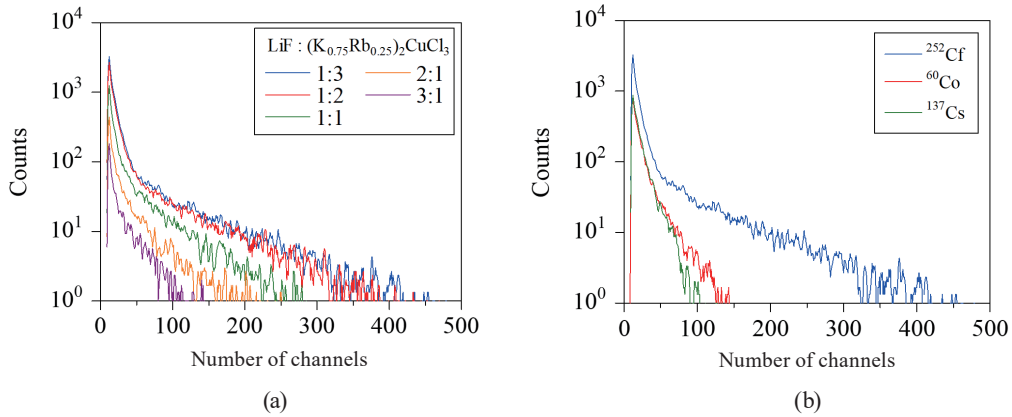

Fig. 3. (Color online) Pulse height spectra of (a) all the obtained samples excited using ^{252}Cf and (b) the 1:3 sample excited using ^{252}Cf, ^{60}Co, and ^{137}Cs.

the intensity of the emission from $(K_{0.75}Rb_{0.25})_2CuCl_3$ becomes low, and many signals should overlap with the thermal noise of the PMT. These signal intensities correspond to a significantly low channel region in the pulse height spectrum (for example, a few channels or less), and although more nuclear reactions should be occurring when the Li content is higher, the pulse count is lower because it is outside the range of the graph.

Figure 4(a) shows the pulse height spectra of the 1:3 sample and Li-glass GS20 under thermal neutron irradiation. The 1:3 sample did not show a full absorption peak because of the characteristics of the opaque composite. Consequently, the light yield could not be estimated accurately. GS20 showed a full absorption peak at around 300 channels, whereas the 1:3 sample had a wide signal intensity distribution from 0 to approximately 450 channels. The emission peak wavelengths of GS20 and $(K_{0.75}Rb_{0.25})_2CuCl_3$ are both approximately 400 nml; therefore, the wavelength dependence of the quantum efficiency (QE) of the PMT does not affect the measurement results. If the light yield of GS20 is 6000 photons/neutron, the signal intensities of the 1:3 sample can be estimated to be equivalent to a light yield of less than 9000 photons/neutron. This may be an underestimated value because the maximum shaping time of the shaping amplifier used was 10 μs, and scintillation decay times of the $(K, Rb)_2CuCl_3$ crystals were 11–13 μs; therefore, scintillation pulses might not have been integrated over the entire range. However, since the difference between the decay time and the shaping time is not large, we believe that the obtained value has sufficient accuracy as a rough estimation.

For comparison, the light yield of a commercial opaque composite, LiF/ZnS:Ag, was also evaluated. Figure 4(b) shows the pulse height spectra of LiF/ZnS:Ag and GS20 under thermal neutron irradiation. Because the applied voltage of the PMT is different between Figs. 4(a) and 4(b), the peak position is also different, and the full absorption peak of GS20 is at approximately 28 channels in Fig. 4(b). The pulse height spectrum of LiF/ZnS:Ag shows a wide signal intensity distribution similar to that of the 1:3 sample, and signals were observed from 0 to approximately 325 channels with the peak at 35 channels. The emission peak wavelength of LiF/ZnS:Ag is 450 nm,[46] and according to the spec sheet of the PMT, the QE of the PMT used in this experiment is 34.34 and 41.01% at 450 and 400 nm, respectively. Therefore, if the light yield of GS20 is 6000

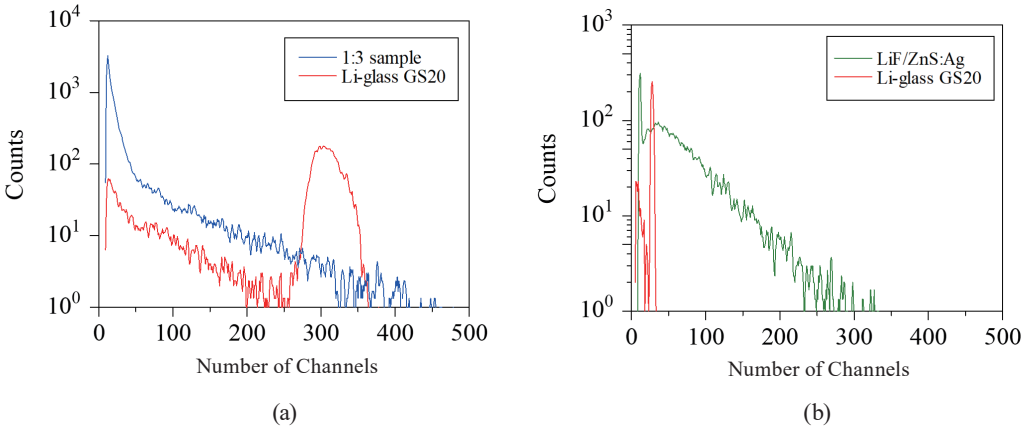

Fig. 4. (Color online) Pulse height spectra of (a) the 1:3 sample and (b) LiF/ZnS:Ag with that of GS20 under thermal neutron irradiation using ^{252}Cf.

photons/neutron,[46] the signals due to LiF/ZnS:Ag can be estimated to be equivalent to the light yield of less than 83000 photons/neutron, and the peak channel corresponds to approximately 9000 photons/neutron. Although Eijk *et al.* reported the light yield of LiF/ZnS:Ag to be 160000 photons/neutron,[46] Wu *et al.* reported that commercial LiF/ZnS:Ag (Eljen Technology, EJ426) showed a light yield of approximately 8000 photons/neutron,[52] which seems to be similar to the peak value in our results. Because LiF/ZnS:Ag cannot show a sharp full absorption peak, the reported light yield values may change depending on the estimation method. Since we estimated light yields of the 1:3 sample and LiF/ZnS:Ag by the same method, we believe the light yield of the 1:3 sample to be at least lower than that of LiF/ZnS:Ag.

To investigate the neutron/γ-ray discrimination capability of the LiF/$(K_{0.75}Rb_{0.25})_2CuCl_3$ composite, the α/β ratio was estimated from Fig. 3(b). Since no full absorption peak or photoabsorption peak were obtained, it is impossible to accurately estimate the α/β ratio. However, the events due to the 4.8 MeV energy of the ^{6}Li(n, α)t reaction appeared at less than 450 channels, and the events due to 0.662 MeV γ-rays from ^{137}Cs appeared at less than 100 channels. Using the upper limit values of these signal intensities, we calculated the α/β ratio to be 0.62, which seemed to be high. For comparison, the pulse height spectra of GS20 and LiF/ZnS:Ag under thermal neutron and γ-ray irradiation were measured. Figure 5(a) shows the pulse height spectra of GS20 excited using ^{252}Cf, ^{60}Co, and ^{137}Cs. Whereas the full absorption peak was observed at 300 channels when using ^{252}Cf, no clear photoabsorption peaks were observed when using both ^{60}Co and ^{137}Cs. However, in the case of using ^{137}Cs, detection events were observed at approximately 150 channels, which is in the region of higher channel number than that of the Compton edge. When using these values, the observed α/β ratio was 0.28. Since the α/β ratio of GS20 has been reported as 0.3,[46] the observed α/β ratio of 0.28 is reasonable. Figure 5(a) shows the pulse height spectra of LiF/ZnS:Ag excited using ^{252}Cf, ^{60}Co, and ^{137}Cs. In the case of LiF/ZnS:Ag, no detection peaks were obtained using either ^{252}Cf, ^{60}Co, or ^{137}Cs owing to the opacity of the composite. Therefore, the α/β ratio cannot be accurately estimated; however, the thermal neutron events appeared at less than 325 channels and the ^{137}Cs γ-ray events

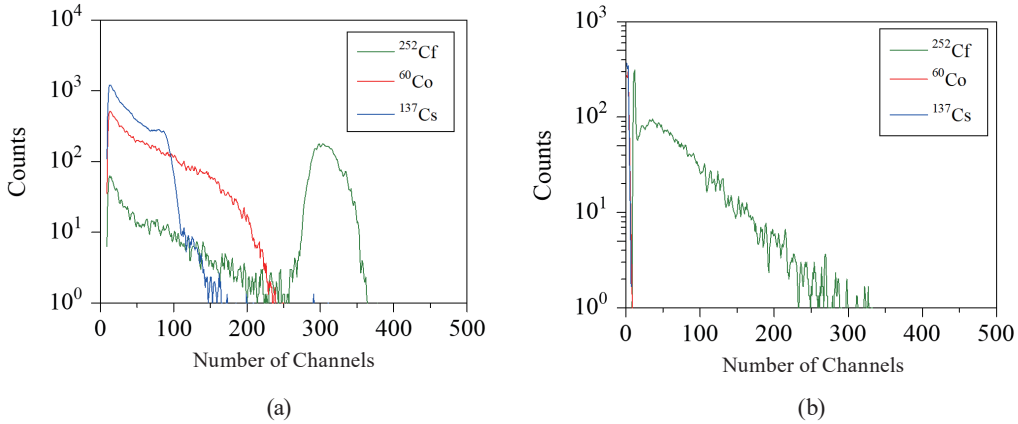

Fig. 5. (Color online) Pulse height spectra of (a) GS20 and (b) LiF/ZnS:Ag excited using ^{252}Cf, ^{60}Co, and ^{137}Cs.

appeared at less than 10 channels. When using these values, the observed α/β ratio was 4.5. Although the estimation method was not clearly shown, the α/β ratio of LiF/ZnS:Ag was reported as 0.44,[46] whereas our observed α/β ratio of 4.5 was significantly higher. In addition, the α/β ratio generally decreases depending on quenching under α-ray excitation, and it should be less than 1. The observed α/β ratio of 4.5 is an unusual value. The reason why this value was obtained is unclear; however, there is the possibility that it is because the absorbed γ-ray energy was low in LiF/ZnS:Ag. It has been reported that the observed α/β ratio of a small piece of the $LiCaAlF_6$:Eu neutron scintillator can be higher than the actual α/β ratio of a large single crystal of $LiCaAlF_6$:Eu because the size of the $LiCaAlF_6$:Eu crystal seems to be smaller than the range of fast electrons induced by γ-rays but larger than the range of high-energy particles produced by ^{6}Li(n, α)t reactions.[53] In the case of the composite neutron scintillators including LiF/ZnS:Ag and LiF/$(K_{0.75}Rb_{0.25})_2CuCl_3$, absorbed γ-ray energies can be low because the thickness of composite scintillators is generally smaller than that of single crystalline scintillators. Therefore, we believe that the observed α/β ratios of the 1:3 sample and LiF/ZnS:Ag were overestimated compared with the actual α/β ratios. However, in practical use, a high observed α/β ratio is an advantage for discrimination between γ-rays and neutrons.

Table 1 shows the summary of observed light yields and α/β ratios of the 1:3 sample, GS20, and LiF/ZnS:Ag. The LiF/$(K_{0.75}Rb_{0.25})_2CuCl_3$ composite can be classified as a similar type of neutron scintillator to LiF/ZnS:Ag. Although its light yield was lower than that of LiF/ZnS:Ag, it has an advantage in terms of a better discrimination capability between γ-rays and neutrons than GS20. The LiF/$(K_{0.75}Rb_{0.25})_2CuCl_3$ composite has a longer decay time of approximately 11–13 μs and a lower light yield than LiF/ZnS:Ag. There is a possibility that these properties are improved by changing the chemical composition of $(K_{0.75}Rb_{0.25})_2CuCl_3$.

Figure 6 shows the temperature dependence of scintillation intensities of the $(K_{0.75}Rb_{0.25})_2CuCl_3$ crystal and GS20 under X-ray irradiation. In the case of LiF/ZnS:Ag, no X-ray-induced scintillation spectrum was observed even at room temperature using this setup, which has a low X-ray detection efficiency. Therefore, only the $(K_{0.75}Rb_{0.25})_2CuCl_3$ crystal and GS20 were evaluated. The relative emission intensity of $(K_{0.75}Rb_{0.25})_2CuCl_3$ decreased more

Table 1
Summary of observed light yields and α/β ratios of the 1:3 sample, GS20, and LiF/ZnS:Ag.

	Light yield (photons/neutron)	Observed α/β ratio	α/β ratio from reference	Reference
1:3 sample	<9000	0.62	N/A	N/A
GS20	6000	0.28	0.3	Ref. 46
LiF/ZnS:Ag	<83000	4.5	0.44	Ref. 46

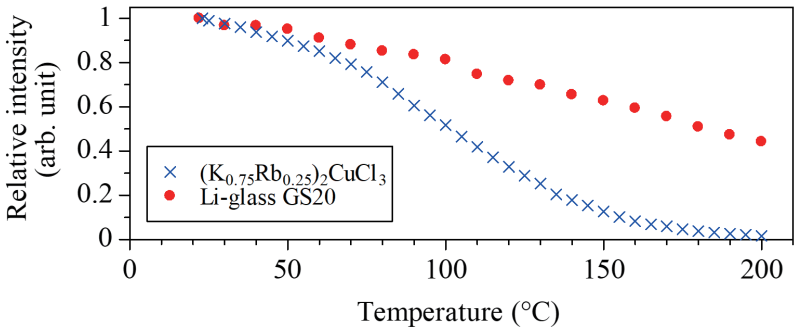

Fig. 6. (Color online) Temperature dependence of scintillation intensities of $(K_{0.75}Rb_{0.25})_2CuCl_3$ and GS20 under X-ray irradiation.

significantly than that of GS20 at high temperatures. It is difficult to use the LiF/$(K_{0.75}Rb_{0.25})_2CuCl_3$ composites for well-logging applications. In contrast, the emission intensity of $(K_{0.75}Rb_{0.25})_2CuCl_3$ was stable at around room temperature. The relative emission intensities of $(K_{0.75}Rb_{0.25})_2CuCl_3$ and GS20 under X-ray irradiation at 40 °C were 94% and 97% of each intensity at room temperature, respectively. The LiF/$(K_{0.75}Rb_{0.25})_2CuCl_3$ composites are acceptable for use at around room temperature.

4. Conclusions

As an application of the $(K, Rb)_2CuCl_3$ crystal, we studied composite neutron scintillators by combining it with LiF at different mixing ratios. We prepared $(K_{0.75}Rb_{0.25})_2CuCl_3$ crystals with high PL quantum yield, which is consistent with the previous study, and formed them into composites. In the PL spectrum of the composite sample, only the emission from the $(K_{0.75}Rb_{0.25})_2CuCl_3$ crystal was observed. Thermal neutrons were successfully detected using the composite samples. Among the samples, those with mass ratios of 1:2 and 1:3 for LiF:$(K_{0.75}Rb_{0.25})_2CuCl_3$ showed the highest light yield (less than 9000 photons/neutron). The observed α/β ratio of the 1:3 sample was 0.62, which indicates that the sample has a high capability of neutron/γ-ray discrimination for practical use. To confirm the performance of $(K_{0.75}Rb_{0.25})_2CuCl_3$ at the high temperatures required for scintillators for well-logging applications, we investigated the emission intensities of X-ray-induced scintillation spectra from room temperature to 200 °C and confirmed that the emission intensity of the $(K_{0.75}Rb_{0.25})_2CuCl_3$ crystal decreased more significantly at high temperatures than that of Li-glass. We concluded that the LiF/$(K, Rb)_2CuCl_3$ composite can be used as a neutron scintillator at room temperature.

The light yield of the sample was lower than that of LiF/ZnS:Ag, and it is currently difficult to use $(K, Rb)_2CuCl_3$ as the alternative to ZnS:Ag; however, we believe that it can be improved by changing its chemical composition.

Acknowledgments

This work was supported by MEXT Grant-in-Aid for Scientific Research A (22H00309), Scientific Research B (21H03736, 22H03872, and 24K03197), and Exploratory Research (22K18997). Asahi Glass Foundation is also acknowledged.

References

1 C. W. E. van Eijk: Nucl. Instrum. Methods Phys. Res., Sect. A **460** (2001) 1. https://doi.org/10.1016/S0168-9002(00)01088-3
2 S. E. Derenzo, M. J. Weber, E. Bourret-Courchesne, and M. K. Klintenberg: Nucl. Instrum. Methods Phys. Res., Sect. A **505** (2003) 111. https://doi.org/10.1016/S0168-9002(03)01031-3
3 T. Yanagida, T. Kato, D. Nakauchi, and N. Kawaguchi: Jpn. J. Appl. Phys. **62** (2023) 010508. https://doi.org/10.35848/1347-4065/ac9026
4 M. Koshimizu: Jpn. J. Appl. Phys. **62** (2023) 010503. https://doi.org/10.35848/1347-4065/ac94fe
5 H. Fukushima, D. Nakauchi, T. Kato, N. Kawaguchi, and T. Yanagida: Jpn. J. Appl. Phys. **62** (2023) 010506. https://doi.org/10.35848/1347-4065/ac9105
6 Y. Fujimoto and K. Asai: Jpn. J. Appl. Phys. **62** (2023) 010605. https://doi.org/10.35848/1347-4065/ac9348
7 D. Nakauchi, T. Kato, N. Kawaguchi, and T. Yanagida: Jpn. J. Appl. Phys. **62** (2023) 010607. https://doi.org/10.35848/1347-4065/ac9181
8 N. Kawaguchi, T. Kato, D. Nakauchi, and T. Yanagida: Jpn. J. Appl. Phys. **62** (2023) 010611. https://doi.org/10.35848/1347-4065/ac99c3
9 D. Yuan, E. G Víllora, N. Kawaguchi, D. Nakauchi, T. Kato, T. Yanagida, and K. Shimamura: Jpn. J. Appl. Phys. **62** (2023) 010614. https://doi.org/10.35848/1347-4065/aca3e5
10 K. Ichiba, T. Kato, D. Nakauchi, N. Kawaguchi, and T. Yanagida: Sens. Mater. **36** (2024) 451. https://doi.org/10.18494/SAM4752
11 T. Kunikata, P. Kantuptim, D.Shiratori, T. Kato, D. Nakauchi, N. Kawaguchi, and T. Yanagida: Sens. Mater. **36** (2024) 457. https://doi.org/10.18494/SAM4754
12 Y. Endo, K. Ichiba, D. Nakauchi, T. Kato, N. Kawaguchi, and T. Yanagida: Sens. Mater. **36** (2024) 473. https://doi.org/10.18494/SAM4758
13 R. Tsubouchi, H. Fukushima, T. Kato, D. Nakauchi, S. Saijo, T. Matsuura, N. Kawaguchi, T. Yoneda, and T. Yanagida: Sens. Mater. **36** (2024) 481. https://doi.org/10.18494/SAM4763
14 H. Fukushima, D. Nakauchi, T. Kato, N. Kawaguchi, and T. Yanagida: Sens. Mater. **36** (2024) 489. https://doi.org/10.18494/SAM4762
15 N. Kawaguchi, N. Hayashi, T. Kunikata, K. Ichiba, T. Kato, D. Nakauchi, and T. Yanagida: Sens. Mater. **36** (2024) 499. https://doi.org/10.18494/SAM4768
16 H. Kimura, H. Fukushima, K. Watanabe, T. Fujiwara, H. Kato, M. Tanaka, T. Kato, D. Nakauchi, N. Kawaguchi, and T. Yanagida: Sens. Mater. **36** (2024) 507. https://doi.org/10.18494/SAM4767
17 K. Miyazaki, D. Nakauchi, T. Kato, N. Kawaguchi, and T. Yanagida: Sens. Mater. **36** (2024) 515. https://doi.org/10.18494/SAM4756
18 K. Yamabayashi, K. Okazaki, D. Nakauchi, T. Kato, N. Kawaguchi, and T. Yanagida: Sens. Mater. **36** (2024) 523. https://doi.org/10.18494/SAM4760
19 H. Fukushima, D. Nakauchi, T. Kato, N. Kawaguchi, and T. Yanagida: Sens. Mater. **35** (2023) 429. https://doi.org/10.18494/SAM4139
20 D. Shiratori, H. Fukushima, D. Nakauchi, T. Kato, N. Kawaguchi, and T. Yanagida: Sens. Mater. **35** (2023) 439. https://doi.org/10.18494/SAM4140
21 P. Kantuptim, T. Kato, D. Nakauchi, T. Kato, N. Kawaguchi, K. Watanabe, and T. Yanagida: Sens. Mater. **35** (2023) 451. https://doi.org/10.18494/SAM4141
22 K. Okazaki, D. Nakauchi, H. Fukushima, T. Kato, N. Kawaguchi, and T. Yanagida: Sens. Mater. **35** (2023) 459. https://doi.org/10.18494/SAM4144

23 A. Ito and S. Matsumoto: Jpn. J. Appl. Phys. **62** (2023) 010612. https://doi.org/10.35848/1347-4065/aca249
24 M. Koshimizu, Y. Fujimoto, and K. Asai: Sens. Mater. **35** (2023) 521. https://doi.org/10.18494/SAM4149
25 T. Kato, D. Nakauchi, N. Kawaguchi, and T. Yanagida: Sens. Mater. **36** (2024) 531. https://doi.org/10.18494/SAM4749
26 Y. Shao, R. L. Conner, N. R. S. Souza, R. S. Silva, and L. G. Jacobsohn: Jpn. J. Appl. Phys. **62** (2023) 010601. https://doi.org/10.35848/1347-4065/ac9941
27 D. Nakauchi, F. Nakamura, T. Kato, N. Kawaguchi, and T. Yanagida: Sens. Mater. **35** (2023) 467. https://doi.org/10.18494/SAM4138
28 T. Kunikata, T. Kato, D. Shiratori, P. Kantuptim, D. Nakauchi, N. Kawaguchi, and T. Yanagida: Sens. Mater. **35** (2023) 491. https://doi.org/10.18494/SAM4145
29 K. Shinozaki, G. Okada, N. Kawaguchi, and T. Yanagida: Jpn. J. Appl. Phys. **62** (2023) 010603. https://doi.org/10.35848/1347-4065/ac95e6
30 N. Wantana, E. Kaewnuam, Y. Tariwong, N. D. Quang, P. Pakawanit, C. Phoovasawat, N. Vittayakorn, S. Kothan, H. J. Kim, and J. Kaewkhao: Jpn. J. Appl. Phys. **62** (2023) 010602. https://doi.org/10.35848/1347-4065/ac9876
31 H. Masai and T. Yanagida: Jpn. J. Appl. Phys. **62** (2023) 010606. https://doi.org/10.35848/1347-4065/ac91b8
32 D. Shiratori, H. Fukushima, D. Nakauchi, T. Kato, N. Kawaguchi, and T. Yanagida: Jpn. J. Appl. Phys. 62, (2023) 010608. https://doi.org/10.35848/1347-4065/ac90a4
33 K. Shinohara, M. J. F. Empizo, M. Cadatal-Raduban, K. Yamanoi, T. Shimizu, M. Yoshimura, N. Sarukura, T. Murata: Jpn. J. Appl. Phys. **62** (2023) 010612. https://doi.org/10.35848/1347-4065/aca0d4
34 D. Nakauchi, H. Kimura, D. Shiratori, T. Kato, N. Kawaguchi, and T. Yanagida: Sens. Mater. **36** (2024) 573. https://doi.org/10.18494/SAM4750
35 Y. Takebuchi, A. Masuno, D. Shiratori, K. Ichiba, A. Nishikawa, T. Kato, D. Nakauchi, N. Kawaguchi, and T. Yanagida: Sens. Mater. **36** (2024) 579. https://doi.org/10.18494/SAM4751
36 K. Okazaki, D. Nakauchi, A. Nishikawa, T. Kato, N. Kawaguchi, and T. Yanagida: Sens. Mater. **36** (2024) 587. https://doi.org/10.18494/SAM4753
37 N. Kawaguchi, K. Watanabe, D. Shiratori, T. Kato, D. Nakauchi, and T. Yanagida: Sens. Mater. **35** (2023) 499. https://doi.org/10.18494/SAM4136
38 Y. Takebuchi, D. Shiratori, T. Kato, D. Nakauchi, N. Kawaguchi, and T. Yanagida: Sens. Mater. **35** (2023) 507. https://doi.org/10.18494/SAM4142
39 H. Kimura, T. Fujiwara, M. Tanaka, T. Kato, D. Nakauchi, N. Kawaguchi, and T. Yanagida: Sens. Mater. **35** (2023) 513. https://doi.org/10.18494/SAM4146
40 R. Nagaoka, N. Kawano, Y. Takebuchi, H. Fukushima, T. Kato, D. Nakauchi, and T. Yanagida: Jpn. J. Appl. Phys. **62** (2023) 010601. https://doi.org/10.35848/1347-4065/ac943d
41 T. Suto, N. Kawano, K. Okazaki, Y. Takebuchi, H. Fukushima, T. Kato, D. Nakauchi, and T. Yanagida: Jpn. J. Appl. Phys. **62** (2023) 010610. https://doi.org/10.35848/1347-4065/ac8f02
42 N. Kawano, M. Koshimizu, G. Okada, Y. Fujimoto, N. Kawaguchi, T. Yanagida, and K. Asai: Sci. Rep. **7** (2017) 14754. https://doi.org/10.1038/s41598-017-15268-x
43 D. Yuan: ACS Appl. Mater. Interfaces **12** (2020) 38333. https://doi.org/10.1021/acsami.0c09047
44 T. Chen, X. Li, Y. Wang, F. Lin, R. Liu, W. Zhang, J. Yang, R. Wang, X. Wen, B. Meng, X. Xu, C. Wang: J. Energy Chem. **79** (2023) 382. https://doi.org/10.1016/j.jechem.2022.12.016
45 K. Yamabayashi, K. Okazaki, D. Nakauchi, T. Kato, N. Kawaguchi, T. Yanagida: J. Lumin. **275** (2024) 120729. https://doi.org/10.1016/j.jlumin.2024.120729
46 C. W. E. van Eijk, A. Bessière, P. Dorenbos: Nucl. Instrum. Methods Phys. Res., Sect. A **529** (2004) 260. https://doi.org/10.1016/j.nima.2004.04.163
47 N. Kawaguchi, T. Kato, D. Nakauchi, and T. Yanagida: Jpn. J. Appl. Phys. **62** (2023) 010611. https://doi.org/10.35848/1347-4065/ac99c3
48 A.R. Spowart: Nucl. Instrum. Methods **75** (1969) 35. https://doi.org/10.1016/0029-554X(69)90644-2
49 A.R. Spowart: Nucl. Instrum. Methods **135** (1976) 441. https://doi.org/10.1016/0029-554X(76)90057-4
50 C.L. Melcher: Nucl. Instrum. Methods Phys. Res. B: Beam Interact. Mater. At. **40–41** (1989) 1214. https://doi.org/10.1016/0168-583X(89)90622-8
51 N. Kawaguchi, G. Okada, K. Fukuda, and T. Yanagida: Nucl. Instrum. Methods Phys. Res. Sect. A **954** (2018) 161518. https://doi.org/10.1016/j.nima.2018.10.196
52 C. Wu, B. Tang, Z.J. Sun, Q. Zhang, Z. Yang, J. Zhang, Y.D. Yang, J.C. Liang, and J.J. Wu: Radiat. Meas. **58** (2013) 128. https://doi.org/10.1016/j.radmeas.2013.04.004
53 D. Sugimoto, K. Watanabe, K. Hirota, A. Yamazaki, A. Uritani, T. Iguchi, K. Fukuda, S. Ishidu, N. Kawaguchi, T. Yanagida, Y. Fujimoto, A. Yoshikawa, H. Hasemi, K. Kino, Y. Kiyanagi: Phys. Procedia **60** (2014) 349. https://doi.org/10.1016/j.phpro.2014.11.047